Photoacoustic imaging of early inflammatory response using gold nanorods

Kang Kim,[a] Sheng-Wen Huang, Shai Ashkenazi, and Matthew O'Donnell
Department of Biomedical Engineering, University of Michigan, Ann Arbor, Michigan 48109

Ashish Agarwal and Nicholas A. Kotov
Department of Chemical Engineering, University of Michigan, Ann Arbor, Michigan 48109

Michael F. Denny and Mariana J. Kaplan
Division of Rheumatology, Department of Internal Medicine, University of Michigan, Ann Arbor, Michigan 48109

(Received 6 March 2007; accepted 1 May 2007; published online 29 May 2007)

Gold nanorods have unusually strong absorption in near infrared, which can be utilized for an optical imaging with nanocolloids. The feasibility of photoacoustic imaging of inflammatory responses using bioconjugated gold nanorods is demonstrated. To target the stimulated cells, gold nanorods were conjugated to anti-intercellular adhesion molecule-1 (ICAM-1) which binds to cell surfaces over expressing ICAM-1. A monolayer of stimulated endothelial cells labeled with bioconjugated gold nanorods was scanned using a high frequency transducer. Photoacoustic images differentiated inflamed cells from control cells and matched well with fluorescence images. This technology may permit identification of critical inflammation sites such as blood vessels.
 [DOI: 10.1063/1.2743752]

Excessive and uncontrolled inflammation plays a key role in a variety of systemic diseases including rheumatoid arthritis (RA), systemic lupus erythematosus, and allergic diseases and a key role in atherogenesis. Furthermore, patients with diseases characterized by chronic systemic inflammation are at risk to develop accelerated atherosclerosis.[1–3] Understanding the correlation between inflammation and atherosclerosis may therefore provide prognostic information of considerable clinical utility.[4]

Most myocardial infarctions occur when a plaque ruptures and a clot forms at the site. Inflammation is believed to be a major factor in plaque rupture, and susceptible plaques tend to have a damaged fibrous cap and numerous resident macrophages. Inflammatory mediators promote the secretetion of various collagenases, which erode the fibrous cap and prevent its repair by smooth muscle cells. Blood that leaks through the damaged cap coagulates quickly, aided by clot promoters produced by T-lymphocytes and foam cells.[5]

Some biomarkers have predictive value for future vascular events among apparently healthy subjects. Prospective epidemiological studies have found increased vascular risk in association with increased basal levels of inflammatory cytokines such as interleukin-6 (IL-6) and tumor necrosis factor alpha (TNFα); cell adhesion molecules such as soluble or membrane-bound ICAM-1, P-selectin, and E-selectin; and acute-phase reactants such as C-reactive protein and fibrinogen. In this study, the adhesion molecule intercellular adhesion molecule-1 (ICAM-1) was chosen as a biomarker of inflammation and activation of endothelial cells (ECs). ICAM-1 is also a strong inflammatory mediator in systemic inflammatory diseases such as RA.[6]

Photoacoustic imaging can be of exceptional value for detection of inflammation and, in particular, the early forms of immune response. It uses rapid thermal expansion induced by absorption of a laser pulse to create acoustic waves that can propagate to a remote acoustic sensor. The distribution of optical absorption within the object can be imaged by reconstructing the detected acoustic field.[7] The contrast of a photoacoustic image can be enhanced using external agents. Gold nanoparticles conjugated with an antibody have been used to enhance optical absorption (and photoacoustic signals) in targeted cancer tissue and provide high contrast for noninvasive cancer imaging.[8–11] In this study, a single layer of stimulated endothelial cells labeled with bioconjugated gold nanorods was scanned.

Human umbilical vein endothelial cells (HUVECs) were maintained on gelatin-coated tissue culture plates in MCDB131 media (Gibco) supplemented with microvascular EC growth factors (Cambrex). Cells were split into a six well plate (0.1×10^6 cells/well, 38 mm in diameter) two days prior to an experiment. Media were changed 24 h after splitting and the cells were left unstimulated or stimulated with the proinflammatory cytokines Interferon-gamma (IFNγ) (200 ng/ml, Peprotech) and TNFα (25 ng/ml, Peprotech) for 16 h. For photoacoustic and fluorescence microscopy measurements, the HUVEC monolayer was washed with cold MCDB131 media. Cells were blocked for 30 min at 4 °C in blocking media [MCDB131 1% bovine serum albumin (BSA) 1% horse serum (HS)]; the blocking solution was removed and the cells were incubated for 1 h at 4 °C with gold nanorod-conjugated anti-ICAM-1 (Biolegend) or isotype control antibody and diluted fivefold with blocking media. The staining solution was removed and the cells were washed with MCDB131. Monolayers were fixed in 4% paraformaldehye in phosphate-buffered saline (PBS) for 1 h at room temperature, then washed and stored in PBS at 4 °C.

To confirm ICAM-1 expression in HUVECs, cells were counterstained for 1 h at room temperature with a fluorescein isothiocyanate (FITC)-conjugated goat antimouse IgG antiserum (0.5 μg/ml) in PBS/1% BSA/1% HS, and the nuclei

[a]Electronic mail: kangkim@umich.edu

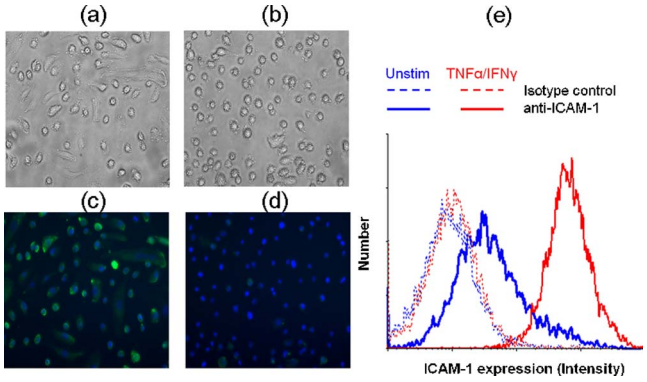

FIG. 1. (Color online) Cell stimulation. Microscope images of (a) stimulated and (b) unstimulated ECs. Fluorescence images of (c) stimulated and (d) unstimulated ECs. ICAM-1 is shown in green and nuclei are in blue. Immunofluorescent measurements were also performed using a flow cytometer (e). ICAM-1 expression reflects that the ECs are well stimulated (red solid line).

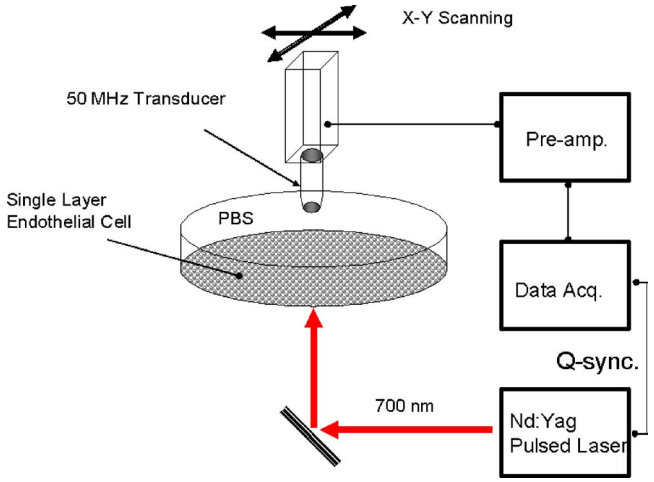

FIG. 2. (Color online) Photoacoustic imaging system.

stained with Hoescht 33342. Fluorescence microscopy was performed using a Leica inverted microscope and acquired images analyzed using ABODE PHOTOSHOP (Fig. 1). All images were acquired and processed using identical settings. From the same batch, a well of unstimulated or stimulated HUVECs was detached from the plate using trypsin/ethylenediaminetetra-acetic-acid (EDTA) solution, incubated for 0.5 h on ice in blocking media, and labeled with unconjugated anti-ICAM-1 or isotype control antibody (1 μg/ml). Labeled HUVECs were washed with MCDB131 then incubated with a FITC-conjugated goat antimouse IgG antiserum (0.5 μg/ml) in PBS. Levels and intensity of ICAM-1 expression were measured using a Coulter Epics XL flow cytometer and analyzed using WINMDI software (version 2.8) (Fig. 1).[12,13]

Gold nanorods of aspect ratio of 3 were synthesized.[14,15] Their optical absorption was centered at 700 nm. Synthesized gold nanorods have a bilayer of surfactant hexadecyltrimethylammonium bromide (CTAB) on their surface acting as a stabilizer to prevent aggregation. After removing excess CTAB, the gold nanorods form a pellet at the bottom of the tube, which was redispersed in de-ionized water.

A layer of polyacrylic acid (PAA) is absorbed on the surface of gold nanorods by adding 1.5 ml of 10 mg/ml PAA solution to 1 ml of gold nanorod solution. Excess PAA in solution was removed. The layer of PAA provides the –COOH functional group required for conjugation. PAA-coated nanorods were dispersed in 1 ml of PBS 6.0 buffer solution followed by the addition of 100 μl of 0.2*M* (*N*-ethyl-*N*′-(3-dimethylaminopropyl)carbodiimide) EDC and 100 μl of 0.2*M* (*N*-hydroxy-succinimide) NHS.[16–20]

After 20 min, the reaction mixture was added to 20 μl of antihuman ICAM-1 or mouse IgG2a. The EDC/NHS mixture forms an active ester intermediate with the gold nanorods which undergoes amidation reaction with the $-NH_2$ group in the anti-ICAM-1 or IgG2a to yield the conjugate. The reaction mixture was refrigerated overnight after removing the unconjugated antibody.

Unstimulated or stimulated ECs were incubated with gold nanorods conjugated to anti-ICAM-1. Additional wells were incubated with gold nanorods alone with no antibody conjugation (blank nanorods). These wells serve as controls to estimate nonspecific binding levels of gold nanorods to cells. The concentration of the gold nanorod solution was 10^{12} particles/ml (10^3 particles/pl) for every case. The plate was then placed in the sample holder of the photoacoustic scanning setup depicted in Fig. 2.

A pulse doubled neodymium doped yttrium aluminum garnet laser (Surelite I-20, Continuum, Santa Clara, CA) pumps an optical parametric oscillator (Surelite OPO Plus, Continuum) to generate 5 ns pulses at 20 Hz with 12 mJ pulse energy. The wavelength was tuned to 700 nm. The laser beam was directed to illuminate from the bottom of the cell culturing well (approximately 4 mJ/cm^2 fluence). A focused ultrasonic transducer ($LiNbO_3$, 50 MHz, $f/1.5$) is used to detect the photoacoustic signal. A motorized *X*-*Y* stage was used to map the photoacoustic signal. For the map of cells bound with bioconjugated nanorods, the step size was 50 μm and the step size was 250 μm for the scan of cells bound with blank nanorods. The photoacoustic signal was averaged eight times at each scanning grid point. The transducer output was amplified (model 5910PR, Panametrics), digitized, and recorded by a digital oscilloscope (WaveSurfer 432, LeCroy Corp. Chestnut Ridge, NY) synchronized to the laser.

Photoacoustic images are presented in Fig. 3. Photoacoustic intensity from the bioconjugated nano rods bound to stimulated cells was 10 dB higher on average than that from unstimulated cells. The photoacoustic intensity was also uniform over an extended scanning region of 2×2 mm^2. Scanned images at three different spots in the same well result in approximately the same average intensity and was uniform. The photoacoustic intensity from both stimulated and unstimulated cells bound with blank nanorods was insignificant compared to that from cells with bioconjugated nanorods. This reflects very low nonspecific binding efficiency of blank gold nanorods to endothelial cells.

The same ECs were then counterstained for 1 h at room temperature with a FITC-conjugated goat antimouse IgG antiserum and nuclei stained with Hoechst 33342. Fluorescence microscopy was performed using identical settings used above (Fig. 3).

The fluorescence intensity of the images differentiate stimulated from unstimulated cells and match well to the photoacoustic images presented in Fig. 3. Gold conjugated isotype control antibody did not show induction of photoacoustic signal upon HUVEC stimulation with TNFα and

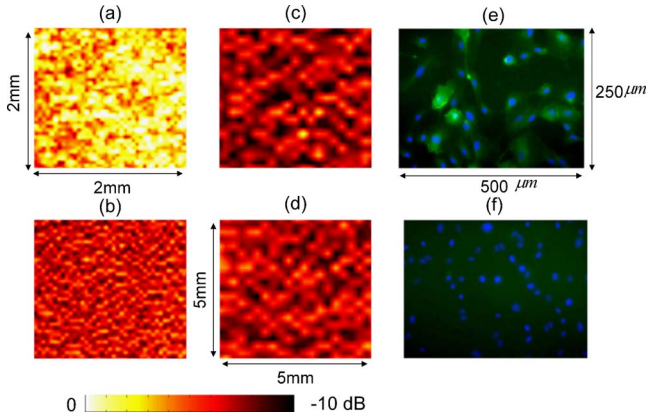

FIG. 3. (Color online) Photoacoustic images of (a) stimulated and (b) unstimulated ECs bound with bioconjugated gold nanorods, and (c) stimulated and (d) unstimulated ECs bound with blank gold nanorods. Note the scanning step was 50 μm for (a) and (b) and 250 μm for (c) and (d). Fluorescence images of the same ECs used for photoacoustic studies were also taken. The brightness of the fluorescent images differentiate (e) stimulated cell from (f) unstimulated cells and match well to the photoacoustic images [(a) and (b)]. Iimages were taken over a 250×500 μm^2 around of the center of the photoacoustic images.

(IFNγ) (not shown), consistent with previous measurements by fluorescence microscopy and flow cytometer shown in Fig. 1.

In summary, the feasibility of molecular imaging of inflammatory responses is demonstrated. Bioconjugated gold nanorod contrast agents targeted stimulated ECs overexpressing ICAM-1 and produced a high contrast for photoacoustic imaging. These images clearly differentiate targeted inflamed cells from control unstimulated ECs. In combination with a commercial ultrasound platform, photoacoustic molecular imaging using gold nanorods as contrast agents can detect inflammatory response at very early stages *in vitro* and, potentially, in vivo. For *in vivo* applications, a proper laser light delivery system synchronized to an ultrasound platform needs to be developed. Minimum detectable gold nanorod concentration by a commercial ultrasound scanner (Sonix RP, Ultrasonix, BC, Canada) was estimated to be about 10^{11} particles/ml (10^2 particles/pl) in a gel phantom (agarose gel mixed with 5% intralipid). The optical absorption coefficient at this concentration is about 0.7 cm^{-1}.

Early detection of inflammation could lead to prompt identification and monitoring of many different diseases. For applications in vascular diseases, light absorption by blood can be a potential problem. The aspect ratio selectivity of gold nanorod absorption spectra will help this issue. In this study, the peak absorption was intentionally selected to be 700 nm where absorption by blood is minimum (~2 cm^{-1}).[21] At this wavelength, light can be delivered to some of the major arteries such as the carotid. Based on the absorption coefficient at minimum detectable concentration above, photoacoustic intensity enhancement of 10 dB can be expected for gold nanorod concentration of about 1.0×10^{12} particles/ml (1.0×10^3 particles/pl). This corresponds to only about 500 nanorods EC of 10 μm in diameter (~0.5 pl). In combination with an optical fiber light delivery system, conventional intravascular ultrasound can also access some other major arteries such as the coronary system.

[1] M. D. Pinkowish and E. A. Amsterdam, Patient Care **39**, 16 (2005).
[2] J. M. Esdaile, M. Abrahamowicz, T. Grodzicky, Y. Li, C. Panaritis, R. du Berger, R. Cote, S. A. Grover, P. R. Fortin, A. E. Clarke, and J. L. Senecal, Arthritis Rheum. **44**, 2331 (2001).
[3] M. J. Kaplan, Curr. Opin. Rheumatol. **18**, 289 (2006).
[4] P. Libby, P. M. Ridker, and A. Maseri, Circulation **105**, 1135 (2002).
[5] P. Libby, Nature (London) **420**, 868 (2002).
[6] P. A. Klimiuk, S. Sierakowski, R. Latosiewicz, J. P. Cylwik, B. Cylwik, J. Skowronski, and J. Chwiecko, Ann. Rheum. Dis. **61**, 804 (2002).
[7] V. E. Gusev and A. A. Karabutov, *Laser Optoacoustics* (American Institute of Physics, New York, 1993).
[8] A. Conjusteau, S. A. Ermilov, D. Lapotko, H. Liao, J. Hafner, M. Eghtedari, M. Motamedi, N. A. Kotov, and A. A. Oraevsky, Proc. SPIE **6086**, 60860K (2006).
[9] P.-C. Li, C.-W. Wei, C.-K. Liao, C.-D. Chen, K.-C. Pao, C.-R. C. Wang, Y.-N. Wu, and D.-B. Shieh, Proc. SPIE **6086**, 60860M (2006).
[10] L. M. Liz-Marzan, Langmuir **22**, 32 (2006); L. M. Liz-Marzan, M. Giersig, and P. Mulvaney, *ibid.* **12**, 4329 (1996).
[11] J. A. Copland, M. Eghtedari, V. L. Popov, N. A. Kotov, N. Mamedova, M. Motamedi, and A. A. Oraevsky, Mol. Imag. Biol. **6**, 341 (2004).
[12] E. M. Shevach, *Immunofluorescence and Cell Sorting, Current Protocols in Immunology* (Wiley, New York, 2002), Chap. 5.
[13] J. Doukas and J. S. Pober, J. Immunol. **145**, 1727 (1990).
[14] B. Nikoobakht and M. A. El-Sayed, Chem. Mater. **15**, 1957 (2003).
[15] C. J. Murphy and N. R. Jana, Adv. Mater. (Weinheim, Ger.) **14**, 80 (2002).
[16] A. Gole and C. J. Murphy, Langmuir **21**, 10756 (2005).
[17] Y. Wang, Z. Tang, and S. Tan, Nano Lett. **5**, 243 (2005).
[18] J. Lee, A. O. Govorov, J. Dulka, and N. A. Kotov, Nano Lett. **4**, 2323 (2004).
[19] S. Wang, N. Mamedova, N. A. Kotov, W. Chen, and J. Studer, Nano Lett. **2**, 817 (2002).
[20] N. N. Mamedova, N. A. Kotov, A. L. Rogach, and J. Studer, Nano Lett. **1**, 281 (2001).
[21] M. Wray, M. Cope, D. T. Deply, J. S. Wyatt, and E. O. R. Reynolds, Biochim. Biophys. Acta **933**, 84 (1988).